Measurement 61 (2015) 206–215

Contents lists available at ScienceDirect

Measurement

journal homepage: www.elsevier.com/locate/measurement

A Low-Cost Flexible-Platform (LCFP) for characterization of photodetectors

J.M. Gomes [a], J.H. Correia [a], J.P. Carmo [b,*]

[a] University of Minho, Dept. Industrial Electronics, Campus Azurem, 4800-058 Guimaraes, Portugal
[b] University of São Paulo (USP), Dept Electrical Engineering (SEL), Avenida Trabalhador São-Carlense, 400, Pq. Ind. Arnold Schimidt, São Carlos-SP CEP 13566-590, Brazil

ARTICLE INFO

Article history:
Received 17 July 2014
Received in revised form 23 September 2014
Accepted 28 October 2014
Available online 6 November 2014

Keywords:
Characterization setup
Photodetectors characterization
CMOS photodetectors

ABSTRACT

This paper presents a Low-Cost Flexible-Platform (LCFP) for measuring and characterizing photodetectors. This LCFP can characterize simultaneously up to 16 photodetectors and is composed by two main electronic circuit boards: a Transimpedance Amplifier Board (TIAB) and a Development Board (DevB). The TIAB was designed and optimized to reduce the noise increase, in order to convert photocurrents into voltages and at the same time, allowing the gain selection between one of the three values: 1×10^5 (low-gain, LG), 1×10^6 (medium-gain, MG) and 1×10^7 (high-gain, HG). The DevB is composed by 16 analog inputs, 54 digital inputs/outputs and an internal Analog to Digital Converter (ADC). It is possible to digitally change the Upper End Voltage (UEV) of the ADC's range to voltages below +5 V. The DevB can convert into the digital domain each one of the 16 analog signals from the TIAB with a resolution of 48.9 nA, 4.9 nA and 0.5 nA for the highest value of UEV (+5 V) and when either LG, MG or HG is selected, respectively. The measured data can be acquired in real-time with *LabView* software, which allows the real-time monitoring of the photocurrents for individual elements in the photodetector both through a numeric and graphical display. The light intensity can be defined by 8 digital outputs allowing 256 light intensity increments/steps from 0 to a maximum defined (by the lamp's manufacturer) light intensity. This LCFP can be used in industry to make quality control, e.g., when different test conditions are applied to the optical sensors/photodetectors and the user/customer need to quickly check if the response or performance is acceptable or resulted on any significant drifts. All these features combined with the low-cost under 1400 € makes this LCFP a suitable tool to quickly evaluate the performance of optical sensors/photodetectors.

1. Introduction

The field of photonics is one that offers the possibility to achieve one of the greatest realizations and applications because the light is present in all aspects of the human life and our way of living was impossible without light. Therefore, the most challenging class of applications is undeniably those one used to detect and/or manipulate the light. There is available a huge number of applications based on light, ranging from medicine [1], chemical analysis for determination of biomolecules [2], biomechanics [3], sensing based on optics [4], imaging [5], spectroscopy [6], laser metrology [7], agriculture [8] and so on. This is not strange when looking back to the second century before our age, when (according to the legend) Archimedes planned to destroy enemy ships using a solar heat ray with an array of actuators to change the shape of a mirror [9].

* Corresponding author.
E-mail address: jcarmo@sc.usp.br (J.P. Carmo).

http://dx.doi.org/10.1016/j.measurement.2014.10.042
0263-2241/

All of these fascinating applications could not be possible without optical components, e.g., optical sources, optical accessories (mirrors, beam-splitters, lenses, prisms, gratings, among others) and optical detectors. These last components are widely referred as photodetectors. A photodetector is a well-known transducer device that can sense light and convert it to an electric current, commonly referred as photocurrent. These types of sensors include for example: photomultiplier tubes [10], photodiodes [11], phototransistors [12], photogates [13] and thermoelectric converters sensible to infra-red (IR) light [14]. Since each application requires different specifications, a compatible photodetector must be selected accordingly. This selection is often determined by the wavelength of the light being detected and photodetector characteristics such as responsivity, sensitivity, response speed, linearity, voltage/current noise, detectivity and also physical dimensions. Moreover, it is crucial to predetermine the generated photocurrent I_L under the application conditions in order to design the electronic reading circuit. In this context, the responsivity R_{ph}, measured in amperes per watt (A/W), is one of the most important photodetector characteristic as it relates the generated current output I_L per optical power input P_O [15,16]. Normally, the responsivity of a photodetector is determined by reading a generated photocurrent in response to an incident light with controllable parameters (e.g., the wavelength, the intensity, or both) into the sensitive active area. The responsivity is then given by $R_{ph}(\lambda) = I_L/P_O$ to highlight the dependence with the wavelength. Another not less important quantitative characteristic of photodetectors is the quantum efficiency $QE(\lambda)$, which reflects the photon-sensitivity of a photodetector as a function of the wavelength of impinging photons [15,16]. In formal terms, the quantum efficiency is given by the ratio between the number of generated electrons N_e and the number of the incident photons N_{ph} in the photodetector [15,16]. In terms of all physical quantities, the quantum efficiency is given by:

$$QE(\lambda) = \frac{N_e}{N_{ph}} = \frac{\left(\frac{I_L}{e}\right)}{\left(\frac{P_O}{h\nu}\right)} \tag{1}$$

where e [C] is the charge of an electron, h is the Planck's constant, and ν is the frequency of the photons in the light. The quantum efficiency can be related with the responsivity, by making a further development of Eq. (1):

$$QE(\lambda) = \frac{I_L}{P_O} \times \frac{h\nu}{e} = R(\lambda) \times \frac{h\nu}{e} \tag{2}$$

from the quantum theory, the energy of a photon is given by $E_{ph} = h\nu = hc/\lambda$, where c is the speed of light. Then, the relation between the responsivity and the quantum efficiency is obtained by replacing the photon's energy in Eq. (2):

$$R(\lambda) = QE(\lambda) \times \frac{e\lambda}{hc} \tag{3}$$

This characterization process must occur in a stable environment offering immunity to external light source interferences and human error, in order to provide accurate and repeatable results. In this context, this paper presents a Low-Cost Flexible-Platform (LCFP) capable to simultaneously measure the photogenerated current of 16 photodetectors. Behind the laboratory environment, an obvious application is in the industry, where customized tool (jigs) is required throughout the manufacturing process in order to perform quality control and to guarantee that a number of products are exactly the same. In conclusion, the Low-Cost and High-Flexibility combined with automated testing and data acquisition under controlled conditions makes this LCFP a functional setup for a wide-range of applications.

2. Design

2.1. System overview

Fig. 1 shows the block diagram of the proposed Low-Cost Flexible-Platform (LCFP). The LCFP is made of two sets of components: the core and the replaceable components. The set forming the core components of the LCFP include a Transimpedance Amplifier Board (TIAB) and a Development Board (DevB). The core components are unchanged from configuration to configuration and are responsible for all the automated acquisition and control process. The set of replaceable components can change according the desired configuration and in its base configuration is composed by a LED-based light source, an optical filter, a beam splitter, a light sensor to measure the light intensity, and a controllable LED driver for dimming the light intensity.

As illustrated in Fig. 1, the light source is comprised by a replaceable Light Emitting Diode (LED) of a known normalized wavelength distribution and by two additional optical accessories: a 600 grit ground glass diffuser and a Ø50.8-*f*60.0 collimation lens.

The optical filter is optional and changeable and can be used to define a precise wavelength impinging both the photodetector(s) under analysis and light sensor.

The emitted light beam travels into a 30:70 (R:T) beamsplitter that splits the light into two light beams: the transmitted, with 70% of the initial light intensity, focuses on the photodetector array being tested; while the second, with 30% of the light intensity, is reflected in a 90° axis, focusing on a luxmeter (the light sensor in Fig. 1). This second light beam enables the feedback reading of the light intensity. The output of the luxmeter is an analog voltage between 0 V and 2 V that is converted into the digital domain by an ADC integrated circuit and further acquired by the Development Board (DevB). The luxmeter works as a light sensor in the base configuration of LCFP due to its low-cost, simplicity of use and interfacing with the DevB. During this process, the TIAB reads the output value of each photodetector current and converts into a correspondent voltage signal. This voltage signal output is also acquired by the DevB that sends both the luxmeter and photodetectors values towards a personal computer. The DevB is also responsible for generating a digital control signal for controlling the light source driver, in order to dimming the intensity of the light produced by this same light source. This process can be either manual or automatically controlled, e.g., working respectively on an

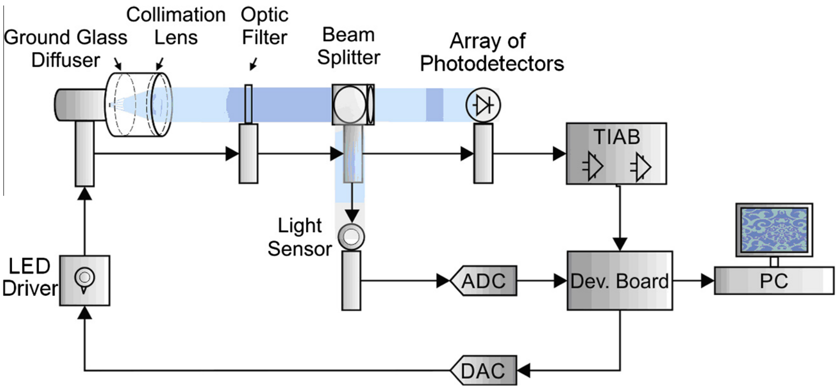

Fig. 1. Block diagram of the proposed setup.

open-loop or on a closed-loop configuration. Additionally, it is advisable to replace the luxmeter by a power meter for an accurate measurement and correction for intensity changes when characterizing photodetectors at different colors. This avoids the need of mathematical corrections, whose errors can result high.

2.2. The Transimpedance Amplifier Board (TIAB)

A photodetector can generate a very small current, in the magnitude of picoamperes or less, when its surface is illuminated by light with energy higher than the bandgap energy of the material [19]. One compatible reading circuit of choice, among several different circuits, is the transimpedance amplifier configuration represented in Fig. 2. This circuit is a current to voltage converter that offers the advantage of low impedance to the photodetector, uniform frequency response for the required bandwidth and adjustable gain by selecting the feedback resistor value accordingly. The governing equation for the gain is $R = V_o/I_i$ where R, V_o and I_i are the resistor that sets the gain, output voltage and the photocurrent respectively.

The TIAB is custom made I/V board and as showed in Fig. 3, it consists of a prototype on a double side printed circuit board to serve as the interface between the photodetectors and the DevB. This board was designed for low-noise operation because the photocurrents are in the range of few nA and must be amplified without degrading the Signal-to-Noise Ratio (SNR). Therefore, it was of major importance to select components with a low Noise Figure (NF) for implementing the first chain of amplifiers.

In the center of Fig. 3(a) there is a 40 pin dual in-line socket (DIL40) connected to four OPA4132 Burr-Brown integrated circuits (IC), where each one offers four operational amplifiers. Each operational amplifiers presents low-noise values of 8 nV/Hz$^{1/2}$ at 1 kHz and a wide bandwidth of 8 MHz. The 16 operational amplifiers are mounted in a way to implement a transimpedance amplifier configuration and offering a total of 16 acquisition channels. Each individual channel offers 3 gain selections of 1×10^5 (low-gain, LG), 1×10^6 (medium-gain, MG) and 1×10^7 (high-gain, HG). The selection of gain (LG, MG and HG) is done by rearranging the on-board jumper configuration, in order to change the parallel equivalent for the feedback resistors (see Fig. 2). The photograph in Fig. 3(b) clearly allows the observation of 4 sets of OPA4132 ICs, referred Amplifiers, as each one with 4 subsets of 3 jumpers to provide Gain Selection for each of the 4 operational amplifiers inside the IC. In the photograph of Fig. 3(b) is also possible to observe the backside of the 40 pin dual in-line socket (DIL40) and the Board Interface, which is composed by a set of connectors to provide physical connection and fixation of the TIAB into the DevB.

Both the positive and negative inputs are virtually connected to the same voltage potential due to the operational amplifier inherent construction. This makes possible to apply an external bias voltage to the photodetectors cathode connected to the negative input by applying a reference voltage to the amplifiers positive input. This selection is provided by rearranging the configuration of the respective jumper. Fig. 4(a) shows a Computer Assisted Design (CAD) model of the TIAB board and its integration with the development board and optical setup, and a detailed view of the interface between the TIAB and the development board. The development board attaches to a custom made acrylic plate securely with bolts and nuts.

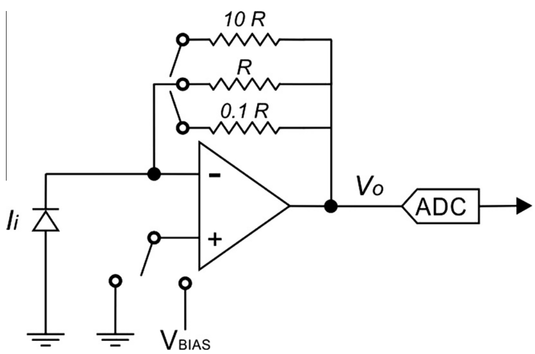

Fig. 2. Transimpedance amplifier configuration and respective electronic for data acquisition.

2.3. Optical system

In Fig. 5(a) is possible to observe a CAD model of this optical system. As in Fig. 5(a), the optical system uses

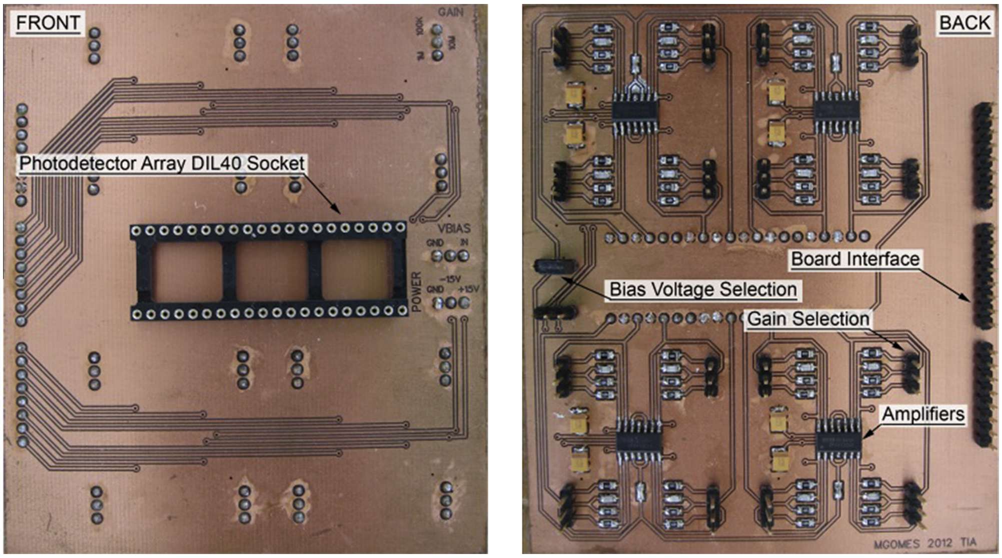

Fig. 3. Photographs of the prototype double (front and nack) side TIAB.

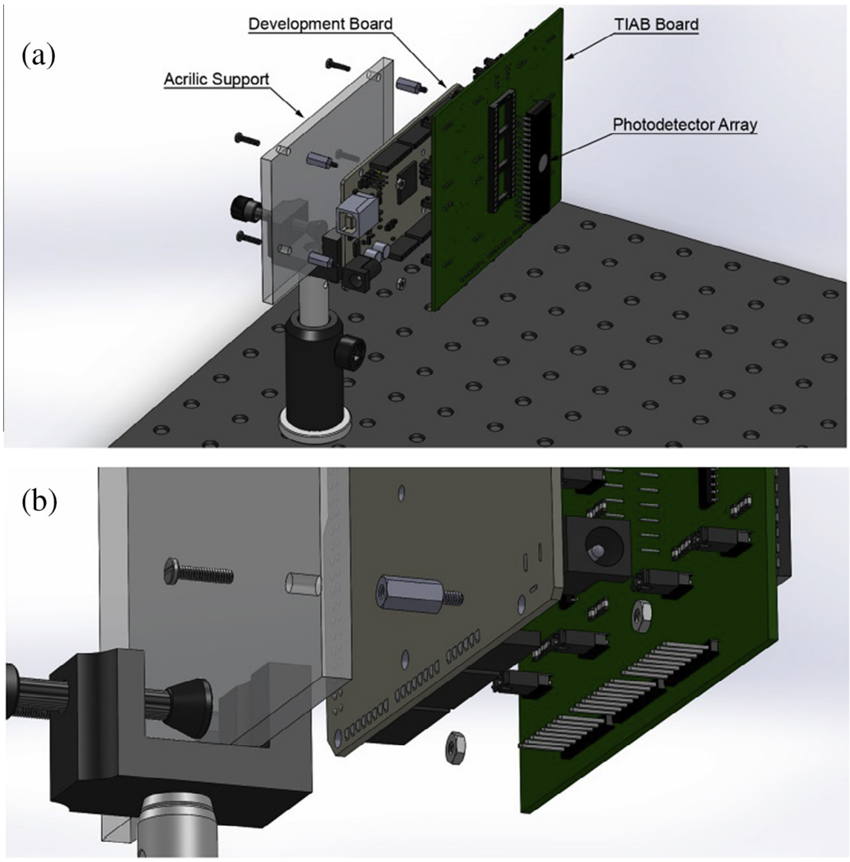

Fig. 4. A CAD model of the TIAB and DevB boards and setup integration: (a) global view; and (b) detailed view of the interface between the TIAB and the DevB and the respective attachment to the acrylic support plate.

low-cost and readily available components off-the-shelf (COTS) with the exception of the custom made TIAB board. This setup is comprised by a dark chamber mounted on a solid perforated aluminum optical base breadboard ensuring immunity to external light sources. The breadboard threaded hole matrix allow for bolt fixated clamping forks

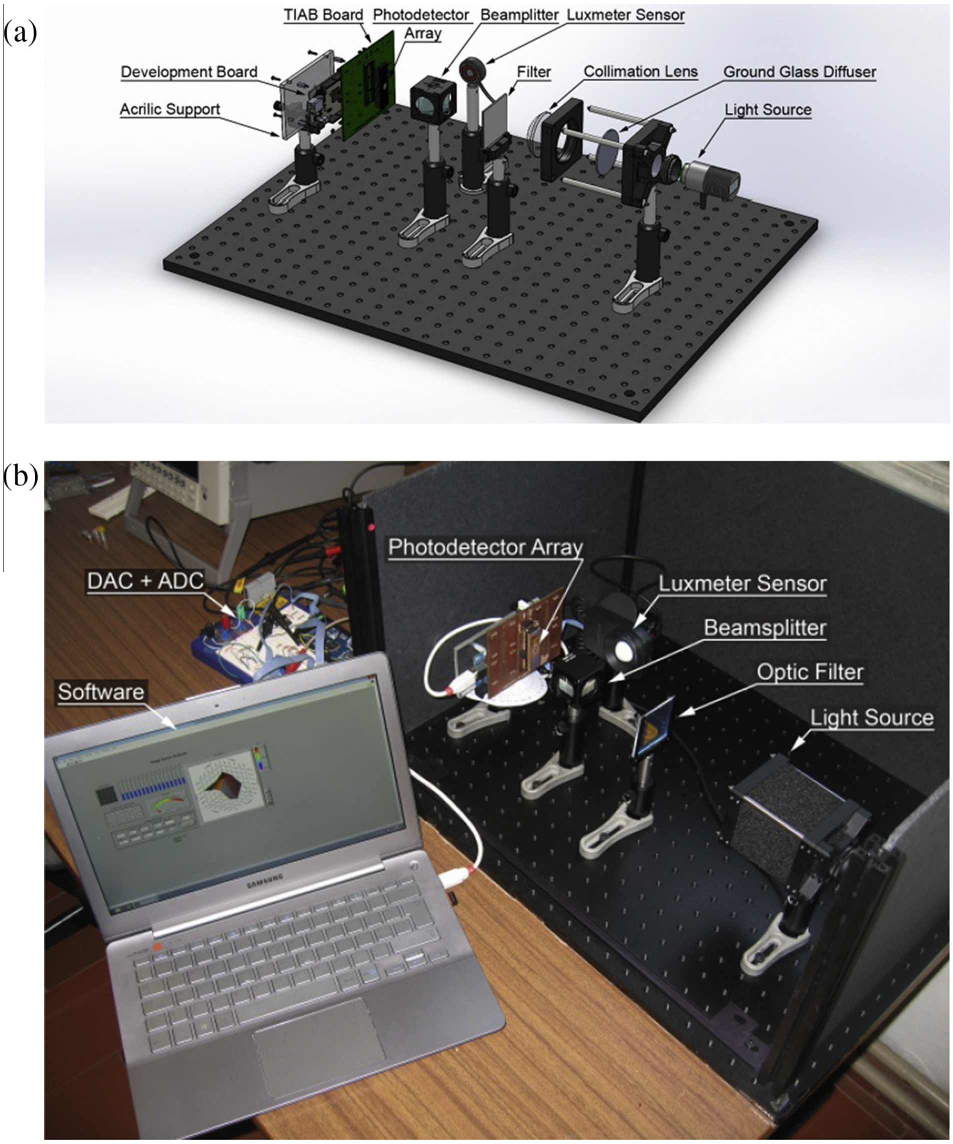

Fig. 5. (a) CAD model of the optical system. (b) Photograph showing the assembled setup with removed front and top cover of the dark chamber.

that secure post holders in place. All the setup components such as filters, light source, beamsplitter, DevB, TIAB and luxmeter sensor are mounted on top of the optical posts and then, inserted into the post holders. The adjustable height and placement allows for a perfect light beam alignment.

The photograph of Fig. 5(b) shows the assembled setup, where it can be observed the TIAB attached into the DevB, which connects to a laptop personal computer through a USB interface. This connection allows a LabView program to control the data acquisition process. In Fig. 5(b) is also possible to observe the perfect aligning of the several parts that compose the optical path from the light source into the photodetectors array and luxmeter sensor.

By using a white light LED light source and optic filters it is possible to obtain light of confined wavelength regions of the visible spectrum in a fast and simple way. A set of 3 dichroic filters for each primary colours (Red, Green and Blue, RGB) can be used to achieve this. The base configuration uses the Thorlab's LED reference MCWHL2 [20] to implement the optical source and the Edmund Optics filters reference 30–634, 46–139 and 30–635 for the Red, Green and Blue filters, respectively [21].

The optical filter holder is placed between the light source and the beamsplitter providing an easy filter interchange. Since the filters offer maximum performance for 0° incident light and to avoid a pronounced Gaussian beam spot distribution leading to an unevenly array lit area, a Ø50.8 mm plano-convex spherical lens with anti-reflex coating for the 350–700 nm wavelengths is used at the focal length distance of 60 mm, and set in place by cage assembly rods. The non-polarizing beamsplitter reference

BS019 from the Thorlabs manufacturer offers minimum beam offset and almost no ghost image and high polarization independency of the incident light.

The used luxmeter (CET CT-1330B High Accuracy Lux Digital Light Meter) follows the CIE 1931 eye sensitivity function $V(\lambda)$ in the photo-optic vision regime which translates the sensitivity of the human eye to the visible light spectrum, peaking at 555 nm wavelength for well-lit conditions [22]. By performing small setup adjustments it is possible to use different reference measurement sensors. By using a luxmeter as the reference sensor it is possible to plot the photodetectors generated current versus illuminance. The main features of this luxmeter include a resolution of 0.1 lx, a measuring range up to 200,000 lx, a repeatability of ±2%, an accuracy of ±3% rdg ± 0.5% of full scale or ±4% rdg ± 10 dgts (for an illuminance smaller or larger than 10^4 lx, respectively). On both cases, the illuminance was calibrated by the manufacturer using a standard incandescent lamp with a temperature of 2856 K. Additionally, it offers a digital display measures are provided on a digital indicator with a resolution of 3 ½ digits.

2.4. Acquisition system

As showed in Fig. 2, each of the 16 outputs in the *I/V* board are connected to the DevB for real-time monitoring. The used DevB was an Arduino™ commercial board, model Arduino Mega 2560 [23], which is based on a microcontroller ATmega2560 [24]. The use of such a DevB simplifies the control and communication with the interface by decentralizing the process of signal acquisition and generation. This board was selected due to its unique characteristics required for implementing a flexible measuring platform. More specifically, the main features of this board includes 54 input/output pins (of which 15 can be used as PWM outputs), 16 analog inputs, 4 UARTs (hardware serial ports), a USB connection to a personal computer running the acquisition/control software (e.g., the *LabView* or a script-based program based in the Arduino software) and four UARTs (Universal Asynchronous Receiver/Transmitter) based on TTL-levels for serial communication. This board also offers a 10 bit analog-to-digital converter (ADC), a serial port for computer communication and a programmable processing unit for managing the samples reading and communication. These 16 analog inputs are compatible with 0–5 V signals which are then converted into the digital domain by the integrated ADC, resulting in a digital signal ranging from 0 to 1023. It is also possible to improve the precision for low excursion analog signals by establishing an external analog voltage reference (AREF): for example, if the input signals do not exceed 2 V, it is possible to use the ADC full range by setting the AREF to 2 V. In this example, the conversion results on a binary representation of 0 and 1023 in binary for 0 and 2 V, respectively. It is also acquired the luxmeter output for every photodetector array measurement in order to correlate both values. Since all the DevB analog inputs are already in use, an external ADC from Texas Instruments with the reference ADC0802 offering 8 bit resolution and parallel interface was used to acquire the luxmeter analog output. The resultant binary word is then acquired by the DevB through the 8 digital inputs.

A computer running a *LabView* program receives the data from the DevB via the serial port. The program interface to the user is presented in Fig. 6, where it is possible to observe 16 photocurrents simultaneously on a bi- and on a tri-dimensional chart. It is necessary to set few parameters in the configuration panel before starting the execution of the software. These parameters include the gain selection of the amplifiers of the *I/V* board, the luxmeter range, the reference voltage used in the DevB integrated ADC, and the serial port related specifications like its selection (and thus, its activation) and baud-rate. It is also possible to select between writing a new data file for each test or append the upcoming data to an existing one. As illustrated in Fig. 6, the data can be visualized at real-time

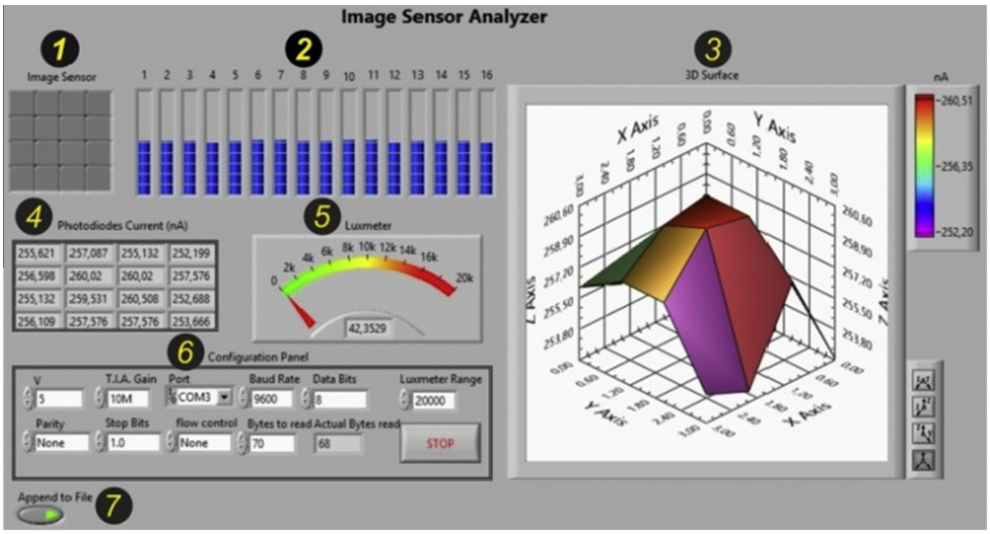

Fig. 6. Program interface for the: 1 – image sensor, 2 – amplifiers output bar graph, 3 – photodetectors relative current output, 4 – photodetectors current output, 5 – luxmeter output, 6 – configuration panel, 7 – data saving selection.

on five indicators: the image sensor array indicator (tag 1 in Fig. 6, e.g., Fig. 6-1) forms a black and white image by converting each individual photodetector output into an image pixel capable of reproducing 255 shades of grey. Next to it, a bar graph display (Fig. 6-2) for each photodetector I/V amplifier assures that the selected gain does not lead to saturation. The table indicator (Fig. 6-4) presents each photodetector output current in nano-amperes (nA), while the luxmeter indicator (Fig. 6-5) shows the current light intensity. It is possible to analyze the photodetectors relative performance in the tri-dimensional chart (Fig. 6-3).

The LED driver used in the light system is the model LEDD1B from Thorlabs which offers a modulation control mode [20]. In this mode, an external voltage signal in the range [0,5] V is used as input signal to control the LED current, and therefore, its brightness. The DevB can generate a pulse-width modulation signal to control the intensity of light. However, an alternative solution was instead considered to avoid the occurrence of flicker in the illumination.

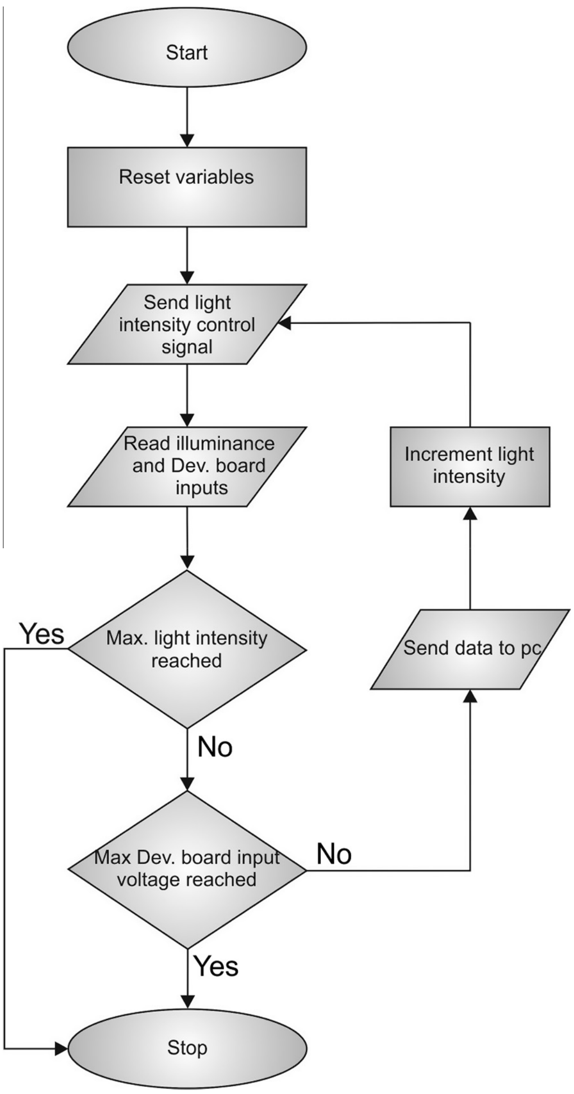

Fig. 7. Light control algorithm.

In this solution, an 8 bit word is generated and converted into the required analog control signal by the 8-bits digital-to-analog converter (DAC), reference TLC7226 from the manufacturer Texas Instruments [25]. This control action in conjunction with the DAC ensures a stable analog control signal across 255 steps, resulting in the same number of stable light intensities. The flowchart in Fig. 7 presents the algorithm to control the light source. This algorithm is implemented on a closed-loop fashion and iteratively optimizes the most suitable illumination and reading range. The first decision consists to determine when the maximum output illumination is generated (e.g., to determine whenever the word 255_{10} is sent on binary into the LED), whereas the second decision consists to determine when the maximum readable illumination by the luxmeter is reached. The second decision must be taken into account because the light intensity increase from this point is useless.

3. Experimental results

3.1. Calibration

The transimpedance amplifier gain is settled by feedbacked resistors. Although the use of high precision resistors guarantees relative accuracy, the resistors production deviations from the desired value leads to an undesired amplifier gain offset. Therefore, each photodetector channel was calibrated against a Keithley Picoammeter model 6487 [14]. This calibration was implemented by software for each one of the 16 channels by using the following procedure: one CMOS photodiode was characterized by the picoammeter and then, by each of the channels for the exact same conditions. The deviation presented by each channel relatively to the picoammeter was then annulled

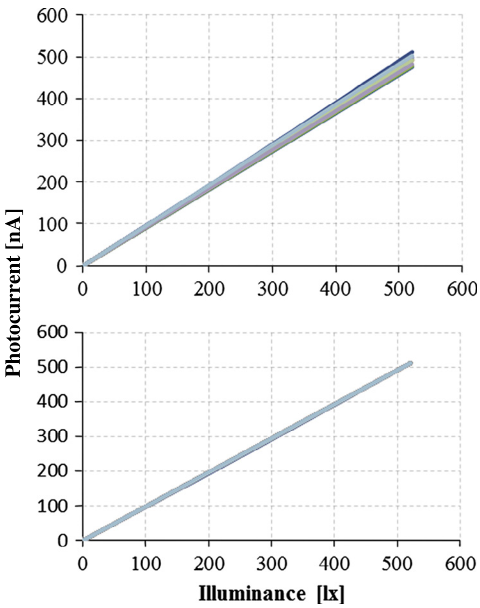

Fig. 8. Channels output before (top plot) and after calibration (bottom plot).

by a multiplying factor that resulted from the division of the picoammeter output by each individual channel outputs. Fig. 8 presents the setup performance before and after calibration, respectively, where it can be observed a performance improvement after the calibration where all the channels produce the same output for the same input.

3.2. Case study 1: CMOS photodiode array

The photocurrent of each of 16 CMOS photodetectors of an imager array arranged in an 8 × 8 matrix was studied for the red, green and blue wavelengths. This array of photodetectors were fabricated in 0.7 µm CMOS on-semiconductor 2-metals/1-poly process [17] and are based on the N+/P-substrate junction. This structure was selected because it provides the best possible quantum efficiency for the visible spectral light range [18]. As demonstrated by Eq. (3), this structure also provides the best possible responsivity and therefore, the best photocurrent. Each individual photodetector is formed by a group of 2 × 2 square photodiodes, with an area of 250 µm × 250 µm, connected in parallel resulting in a total area of 0.25 mm^2 each. Fig. 9(a) shows a photograph of the studied photodetector array encapsulated in a 40 DIL package. The close-up image shows the array in more detail where it can be seen a highlighted area of 2 × 2 photodiodes arrangement resulting in one photodetector.

The photodetectors response for the red, green and blue light wavelengths is showed in Fig. 10(a). Since the response obtained for each individual CMOS photodetector was equal for the same wavelength, each curve characterizes all the 16 CMOS photodetectors presented in the array. This was expected since they all have the exact same characteristics both in size and fabrication process. For the same illuminance values and light source used, the photodetector array revealed higher output values for the blue wavelength, followed by the red and then the green, which required 8 times the blue wavelength illuminance to equal its output response.

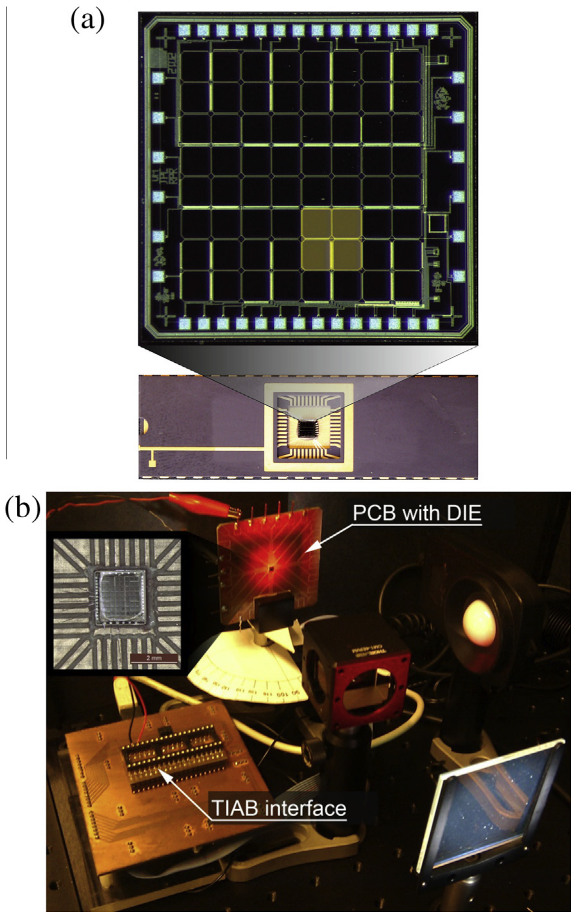

Fig. 9. (a) Image of the photodetector array encapsulated in a DIL40 package. The highlighted zone in the zoomed area illustrates 2 × 2 photodiode arrangement that forms one photodetector. (b) TiaB interface for reading a single photodiode in a DIE and respective zoom detail.

3.3. Case study 2: multiple size CMOS photodiodes

By attaching individual photodetectors directly into the DIL40 socket or using an adaptor it is possible to read the output of unpackaged dies and single photodetectors. Fig. 9(b) shows an unpackaged die with CMOS photodiodes of 500 µm × 500 µm, 500 µm × 250 µm, 250 µm × 250 µm and 25 µm × 25 µm. Fig. 10(a) shows a photodiode response for the red, green and blue wavelengths, while Fig. 10(b) shows the response to 0–2000 lx white light for photodiodes of multiple sizes.

3.4. Case study 3: bias voltage

In some cases, it is mandatory to apply a bias voltage to the photodetector in order to maximize the photogenerated

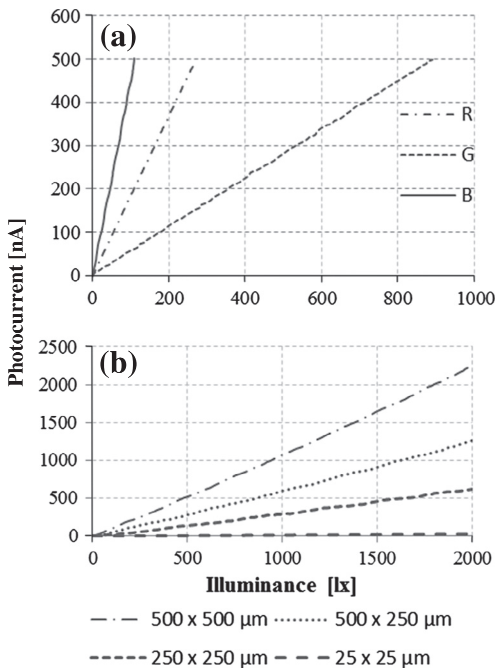

Fig. 10. (a) CMOS photodetector response for the red (R) green (G) and blue (B) wavelengths. (b) Response of multiple photodiodes to 0–2000 lx white light.

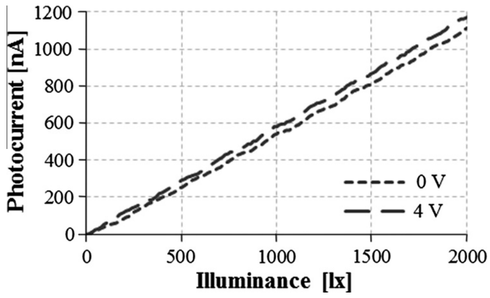

Fig. 11. A 500 μm × 500 μm CMOS photodiode response for the green wavelength with 0 V and −4 V bias voltages.

Table 1
Cost of the assembled setup.

Optical components	709 €
Hardboard sliding door enclosure	173 €
Aluminum breadboard	365 €
Dev. board	35 €
ADC, DAC	10 €
TiaB board	50 €
Luxmeter	50 €
Total	1392 €

current. A CMOS photodiode is created by doping silicon, which is an element from group IV of the periodical table therefore presenting four covalent electrons, with elements from group III and from group V, creating a p-type and a n-type semiconductor respectively. In the neutral zone around the junction between these two types of semiconductors a depletion region is created and the subsequent electric field is originated forcing the electrons-holes pairs to move in opposite ways. When photons carrying energy equal or higher than the bandgap energy reach the depletion zone, where the majority of electron–hole pairs are created, free electrons are attracted by the n-type region thus creating photocurrent. By applying a bias voltage, this depletion zone is enhanced and more electron–hole pairs are created resulting in intensified photocurrent [26].

Fig. 11 shows the response of a 500 × 500 μm^2 CMOS photodiode with a bias voltage of 0 V and −4 V for the green wavelength. The result shows that for the same luminance values the photodiode produces ≈8.56% more photocurrent when a bias voltage of −4 V is applied compared to a bias voltage of 0 V.

4. Conclusions

This paper has presented a Low-Cost Flexible-Platform (LCFP) for characterization of photodetectors. Table 1 resumes the total cost for the major components. By using low-cost and commercial off-the-shelf (COTS) components it is possible to rapidly evaluate the response of photodetectors under static and dynamic luminance values in restricted conditions. Adding to these characteristics, the modularity offered by the setup ensures an easy reconfiguration of the setup and allows its further scalability, (e.g. the adding/replacement of new functions). This LCFP can be used as a customized tool (jigs) in the industry to make quality control throughout the manufacturing process in order to perform quality control, especially when different test conditions are applied and the user/customer need to quickly check if the response or performance is acceptable or has had any significant drift after the tests. Additionally, for all of these considerations, this LCFP is also qualified for academic learning purposes.

Acknowledgements

This work was sponsored by the Brazilian agency National Council of Scientific Research (*Conselho Nacional de Desenvolvimento Científico e Tecnológico, CNPq*) under the grant 400110/2014-8: *Ciência sem Fronteiras/Chamada de projetos* MEC/MCTI/CAPES/CNPQ/FAPS – *Bolsa Pesquisador Visitante Especial* (PVE) 2014.

References

[1] S. Zhang, Q.X. Chen, J.W. Luo, J. Ba, A fast surface reconstruction method for fluorescence molecular tomography based on cross-beam edge back projection, Measurement 46 (2013) 1565–1571.
[2] G. Hui, Y. Zhang, F. Cui, G. Qu, Determination of protein with thioguanine (6-TG) as a probe by synchronous fluorescence technique, Measurement 46 (2013) 1507–1511.
[3] I. Stančić, J. Musić, V. Zanchi, Improved structured light 3D scanner with application to anthropometric parameter estimation, Measurement 46 (2013) 716–726.
[4] H. Guillemain, M. Rajarajan, Y.-C. Lin, C.-T. Chen, T. Sun, K.T.V. Grattan, Feasibility studies using thin sol–gel films doped with a novel lead-selective fluorophore for optical fibre sensing applications, Measurement 46 (2013) 2971–2977.
[5] T.K. Bera, J. Nagaraju, Studies on thin film based flexible gold electrode arrays for resistivity imaging in electrical impedance tomography, Measurement 47 (2014) 264–286.
[6] Y.-Y. Ji, Z.-M. Zhao, R.-D. Ji, L.-X. Wang, Effects of typical food additives on the absorption spectrum properties of black tea, Measurement 49 (2014) 351–357.
[7] S. Yin, Y. Ren, Y. Guo, J. Zhu, S. Yang, S. Ye, Development and calibration of an integrated 3D scanning system for high-accuracy large-scale metrology, Measurement 54 (2014) 65–76.
[8] S.K. Chatterjee, S. Ghosh, S. Das, V. Manzella, A. Vitaletti, E. Masi, L. Santopolo, S. Mancuso, K. Maharatna, Forward and inverse modelling approaches for prediction of light stimulus from electrophysiological response in plants, Measurement 53 (2014) 101–116.
[9] T. Bifano, MEMS deformable mirrors, Nat. Photonics 5 (2011) 21–23.
[10] T. Bezboruah, K. Boruah, P.K. Boruah, An improved resistive amplification network for fast timing photomultiplier tubes, Measurement 37 (2005) 131–134.
[11] Z. Ahmad, S.M. Abdullah, K. Sulaiman, Bulk heterojunction photodiode: to detect the whole visible spectrum, Measurement 46 (2013) 2073–2076.
[12] P. Kostov, W. Gaberl, H. Zimmermann, High-speed bipolar phototransistors in a 180 nm CMOS process, Opt. Laser Technol. 46 (2013) 6–13.
[13] T. Tokuda, T. Noda, K. Sasagawa, J. Ohta, Optical and electric multifunctional CMOS image sensors for on-chip biosensing applications, Materials 4 (2011) 84–102.
[14] T. Brestovič, N. Jasminská, M. Čarnogurská, M. Puškár, M. Kelemen, M. Fil'o, Measuring of thermal characteristics for Peltier thermopile using calorimetric method, Measurement 53 (2014) 40–48.
[15] N. Xie, Low-Power Low-Noise CMOS Imager Design: In Micro-Digital Sun Sensor Application, PhD Thesis, Technical University of Delft (TU-Delft), TU Delft Press, The Netherlands, 2012.
[16] Y. Chen, Low-Noise CMOS Image Sensors for Radio-Molecular Imaging, PhD Thesis, Technical University of Delft (TU-Delft), TU Delft Press, The Netherlands, 2012.
[17] Europractice IC Service: low-cost ASIC prototyping (MPW) and small-medium volume production, 0.7 μm CMOS on-semiconductor (formerly AMI Semiconductor) 2-metals/1-poly process, C07-D0.7 μm option. <http://www.europractice-ic.com/technologies_AMIS_tech.php>.

[18] J.G. Rocha, C.G.J. Schabmueller, N.F. Ramos, S. Lanceros-Mendez, M.V. Moreira, A.G.R. Evans, R.F. Wolffenbuttel, J.H. Correia, Comparison between bulk micromachined and CMOS X-ray detectors, Sens. Actuators A 115 (2004) 215–220.
[19] I. Kenyon, The Light Fantastic: A Modern Introduction to Classical and Quantum Optics, second ed., Oxford University Press, Oxford, 2011.
[20] Thorlabs GmbH, Germany. <http://www.thorlabs.de/>.
[21] Edmund Optics Ltd., UK. <http://www.edmundoptics.co.uk/>.
[22] CIE Proceedings 1, Bureau Central de la CIE, Sec. 4, 3, Paris 1951, pp. 37.
[23] Arduino Mega 2560, Arduino™. <www.arduino.cc>.
[24] ATmega2560 microcontroller, Atmel Corporation. <www.atmel.com/devices/atmega2560.aspx>.
[25] TLC7226, 8-Bit, 5 µs Quad DAC, Parallel Input, Single/Dual Supply, Texas Instruments. <www.ti.com/product/tlc7226>.
[26] X. Wang, Noise in Sub-Micron CMOS Image Sensors, PhD Thesis, Technical University of Delft (TU-Delft), TU Delft Press, The Netherlands, 2008.